

# Peptidoglycan Remodeling and Conversion of an Inner Membrane into an Outer Membrane during Sporulation

Elitza I. Tocheva,<sup>1</sup> Eric G. Matson,<sup>2</sup> Dylan M. Morris,<sup>1</sup> Farshid Moussavi,<sup>4</sup> Jared R. Leadbetter,<sup>2</sup> and Grant J. Jensen<sup>1,3,\*</sup>

<sup>1</sup>Division of Biology

<sup>2</sup>Ronald and Maxine Linde Center for Global Environmental Science

<sup>3</sup>Howard Hughes Medical Institute

California Institute of Technology, Pasadena, CA, 91125, USA

<sup>4</sup>Department of Electrical Engineering, Stanford University, Stanford, CA, USA

\*Correspondence: jensen@caltech.edu

DOI 10.1016/j.cell.2011.07.029

## SUMMARY

Two hallmarks of the *Firmicute* phylum, which includes the *Bacilli* and *Clostridia* classes, are their ability to form endospores and their “Gram-positive” single-membraned, thick-cell-wall envelope structure. *Acetonema longum* is part of a lesser-known family (the *Veillonellaceae*) of *Clostridia* that form endospores but that are surprisingly “Gram negative,” possessing both an inner and outer membrane and a thin cell wall. Here, we present macromolecular resolution, 3D electron cryotomographic images of vegetative, sporulating, and germinating *A. longum* cells showing that during the sporulation process, the inner membrane of the mother cell is inverted and transformed to become the outer membrane of the germinating cell. Peptidoglycan persists throughout, leading to a revised, “continuous” model of its role in the process. Coupled with genomic analyses, these results point to sporulation as a mechanism by which the bacterial outer membrane may have arisen and *A. longum* as a potential “missing link” between single- and double-membraned bacteria.

## INTRODUCTION

For decades bacteria have been classified into two main groups by whether or not they retain crystal violet, the so-called “Gram” stain. Gram-positive cells have a single membrane and a thick peptidoglycan (PG) cell wall, which retains the stain, whereas Gram-negative cells are enclosed by two membranes separated by a thin layer of PG, which does not retain the stain. While more recently the terms Gram “positive” and “negative” have fallen out of favor in the face of richer phylogenetic distinctions, the presence of either one or two enclosing membranes remains a fundamentally intriguing difference between bacterial species. Transport across the inner membrane (IM) of double-membraned bacteria and the single membrane of single-

membraned bacteria is tightly regulated, as these membranes sustain proton gradients essential for metabolism. Outer membranes (OMs) of double-membraned bacteria are structurally and functionally quite different, containing large amounts of the immunologically important macromolecule lipopolysaccharide (LPS, or “endotoxin”) and numerous beta-barrel protein porins that allow passive diffusion of small molecules. Assuming that the first cells were enclosed by a single membrane, it is unclear how and why second membranes evolved (Bos et al., 2007; Lake, 2009).

In the original bacterial classifications, Gram positives were assigned to the phylum *Firmicutes*. Many species of the bacterial phylum *Firmicutes* respond to adverse growth conditions by forming endospores (Piggot and Hilbert, 2004). Sporulation begins with DNA replication, chromosome segregation and packing, asymmetric positioning of the Z ring, and septation (reviewed in Margolin, 2002). This yields a mother cell and a daughter cell, or “prespore,” that are separated by a double-membraned septum. After septum formation, the mother cell engulfs the prespore in a process morphologically similar to phagocytosis. Inside the mother cell, the forespore matures, adding several layers of a protein coat and in some species an exosporium. Finally, when the mother cell lyses, the mature spore is released. These resting forms can remain viable for thousands of years without water or nutrients and can resist, among other environmental insults, ultraviolet (UV) irradiation, heat, pH extremes, and oxidative damage (Setlow, 2007). When favorable conditions return, the spores germinate and new progeny emerge via outgrowth.

For decades, the model organism for studying both sporulation and the “Gram-positive” cell type has been the bacterium *Bacillus subtilis*. *B. subtilis* was the first sporulating bacterium to have its genome sequenced and in many ways is an excellent model organism. Its natural competency has facilitated genetic and biochemical characterization, and its large size has benefited traditional electron microscopy (EM) and light microscopy (LM) investigations. Largely because in EM images of sporulating Gram-positive cells the septum was clearly thinner than the thick, vegetative cell wall (Bechtel and Bulla, 1976), it has long been thought that any PG present in the septum is degraded

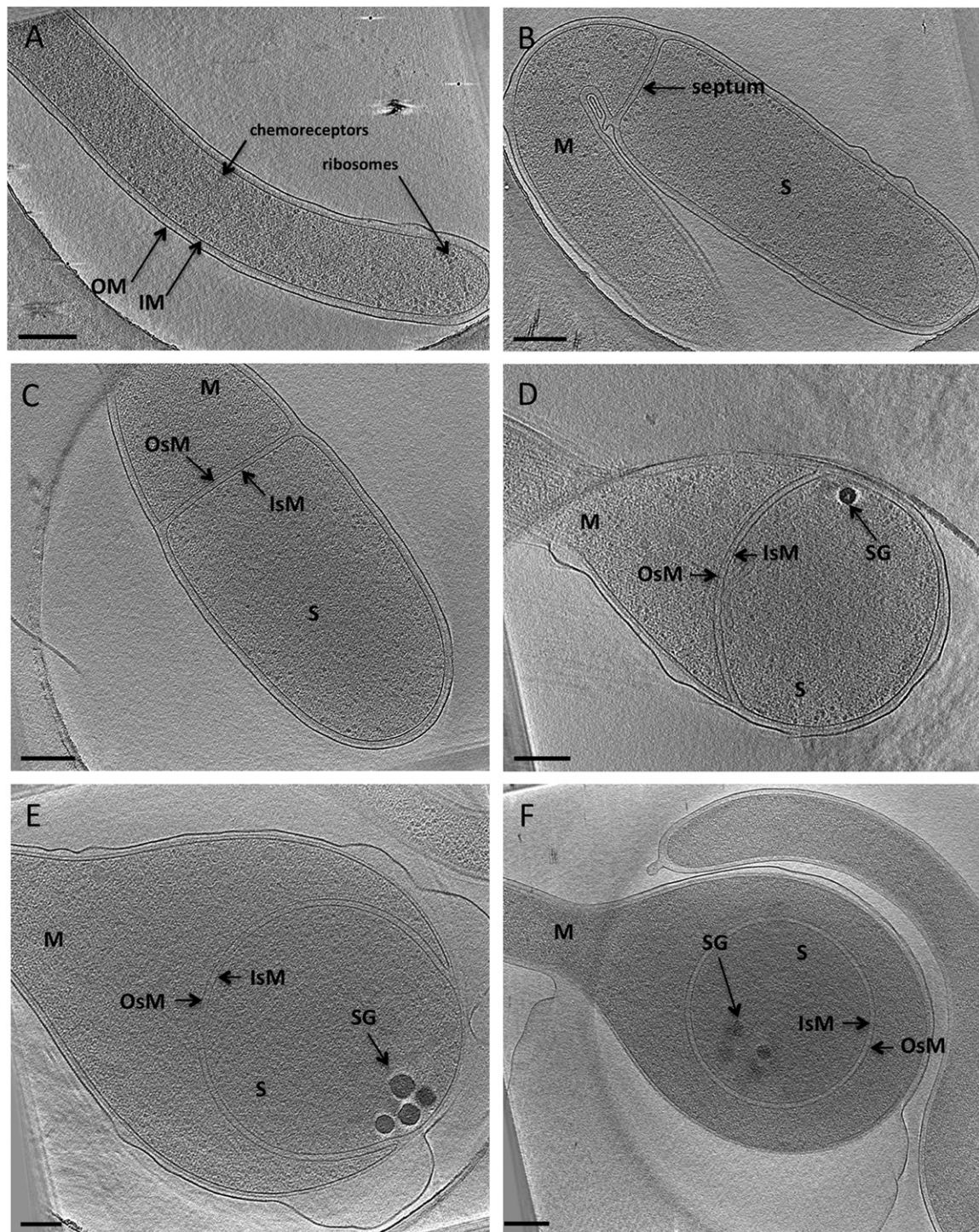


**Figure 1. Stages of Sporulation in *A. longum***

(A) A vegetative cell showing typical Gram-negative cell-wall architecture.

(B) A sporulative septum separates the mother cell (M) from the prespore (S). The septum is formed from the inner membrane (IM) of the mother cell.

(C) The diameter of the prespore enlarges before engulfment, and the septum eventually turns into the inner spore membrane (IsM) and the outer spore membrane (OsM) of the prespore.

(D) Engulfment begins as the IsM and OsM curve and move along the mother cell wall. Storage granules appear at the leading edges of the engulfing membranes (SG, black bodies).

(E) The prespore continues to enlarge and eventually becomes spherical. The number and size of SGs increases as engulfment proceeds.

before engulfment begins. Furthermore, little attention was paid to the fate of the outer spore membrane, since it was not part of the future germinating cell.

*Acetone* *longum* is part of a lesser-known family of the *Firmicutes* (the *Veillonellaceae*), which form endospores but are surprisingly “Gram negative”: they stain Gram negative, they are enveloped by two membranes and a thin cell wall, and their OM contains LPS (Hofstad, 1978; Hofstad and Kristoffersen, 1970; Kane and Breznak, 1991; Mergenhagen, 1965; Rainey, 2009). Like *B. subtilis*, *A. longum* forms endospores that are both pasteurization resistant and calcium dipicolinate containing (Kane and Breznak, 1991). Germination results, however, in a double-membraned, Gram-negative cell, calling attention to the origin of the OM and the periplasmic PG.

Also unlike *B. subtilis*, *A. longum* cells are slender enough to image intact in a near-native state by electron cryotomography (ECT). Previous images of *B. subtilis* and other sporulating cells were obtained by chemical fixing, dehydration, plastic embedding, sectioning, and staining of the samples. Such approaches sometimes fail to preserve important details or even introduce misleading artifacts (Pilhofer et al., 2010). ECT involves neither plastic embedding nor staining, yielding “macromolecular” resolution, three-dimensional (3D) images of biological samples in near-native, frozen-hydrated states (Ben-Harush et al., 2010; Li and Jensen, 2009). ECT has been used for example to identify the architectures of the bacterial flagellar motor and chemoreceptor arrays (Briegel et al., 2009; Chen et al., 2011; Liu et al., 2009).

In this study, we imaged vegetative, sporulating, and germinating *A. longum* cells and endospores with ECT. ECT analyses were supplemented with LM, immunofluorescent labeling, western blotting, traditional EM, mass spectrometry, genome sequencing, and phylogenetic profiling. The images and analyses show that a thin PG layer persists in the septum throughout sporulation and germination, that a protein coat (likely SpoIVA) forms densely packed concentric rings on the mother side of the engulfing septum, and that a region of the IM of the mother cell is inverted and transformed to become the OM of the outgrowing cell. *A. longum*'s peculiar characteristics as an endospore-forming Gram-negative cell suggest possible explanations for the evolution of all *Firmicutes* and the bacterial OM.

## RESULTS

### Vegetative Cell Ultrastructure

The life cycle of *A. longum* cells was studied first by LM. Two vegetative morphologies were observed: flexible rods between 50 and 70  $\mu\text{m}$  in length and rigid rods less than 10  $\mu\text{m}$  in length (Figure S1 available online). The shorter form was observed as cultures entered stationary phase and was the form that produced endospores. Crystal violet was not retained at any time during the life cycle, establishing at least by the simple definition that *A. longum* cells are Gram negative (data not shown).

Ultrastructural ECT studies (Figures 1A–1E, 2A–2E, and 3A–3E; Movie S1 and Movie S2) revealed that the cell envelope of vegetative cells comprised an IM, periplasm, and an OM typical of other Gram-negative bacteria (Figure 1A) (Briegel et al., 2006; Komeili et al., 2006). Closer inspection of the periplasmic space (28 nm wide) revealed the presence of two to three PG-like periplasmic layers  $\sim 2$  nm thick equally spaced 6 nm apart (peak to peak, as all other measurements reported below) (Figure 3A and Figure S3A). These multiple layers appeared similar to one another and were consistently present in the  $\sim 200$  vegetative cells imaged. In areas where the OM was distended, the periplasmic layers remained associated with the IM, suggesting that the layers were more closely associated with the inner rather than the outer membrane.

### Vegetative Septa

Two different types of septa were observed by ECT (Figures S1F and S1G). While vegetative septa occurred at  $\sim 10$   $\mu\text{m}$  intervals along the long, flexible cells, sporulation septa were observed at the tips ( $\sim 1.5$   $\mu\text{m}$  away from the poles) of the short (10  $\mu\text{m}$ ), straight cells. Vegetative septa were smaller than sporulation septa, and while the OMs surrounding vegetative septa ingressed, those surrounding sporulative septa remained flat (Figure 1B and Figure S1G).

### Sporulation

Sporulation begins as the IM invaginates in a ring and constricts until a closed septum is formed across the cell, separating the prespore from the mother cell. Despite repeated attempts, we were unable to find cells exhibiting partial septa, suggesting that septum formation in *A. longum* is rapid. Figure 1B shows a complete sporulative septum accompanied by a minor enlargement in the diameter of the prespore (prespore calculated volume of  $0.22 \pm 0.07$   $\mu\text{m}^3$ , Table S1). PG-like layers were also seen in the septum (Figure S3B). Closer inspection of the junction between the septum and the mother cell wall revealed that the innermost periplasmic layer of the mother cell was continuous with the septal layers (Figures 3B–3D). As sporulation proceeded, the diameter of the spore continued to increase until it was two to three times the diameter of a vegetative cell. In addition, small dense bodies (likely storage granules) were formed at the leading edges of the engulfing membranes (Figures 1D and 3C). Interestingly, the number and size of the storage granules (SGs) in the prespore increased as engulfment proceeded, reaching a final number of eight to 12 per spore, with diameters ranging from 40 to 120 nm and together accounting for  $\sim 7\%$  of the forespore volume (Figure 1E and 3D).

As engulfment proceeded, the edge of the septum moved toward the spore pole along the sides of the mother cell wall. Our tomograms and volume calculations revealed that even though the shape of the prespore changed from cylindrical to spherical, the volume increase was slight (Table S1 and Movie S2). Fusion of the leading edges of the engulfing membranes

(F) Engulfment is completed and a forespore surrounded by an IsM and an OsM is formed in the middle of the mother cell. Each panel is a 20 nm thick tomographic slice through a 3D reconstruction of an intact cell.

Scale bars represent 200 nm (note E and F are slightly smaller scale to show the entire cell pole). See also Figure S1, Table S1, and Movie S1.

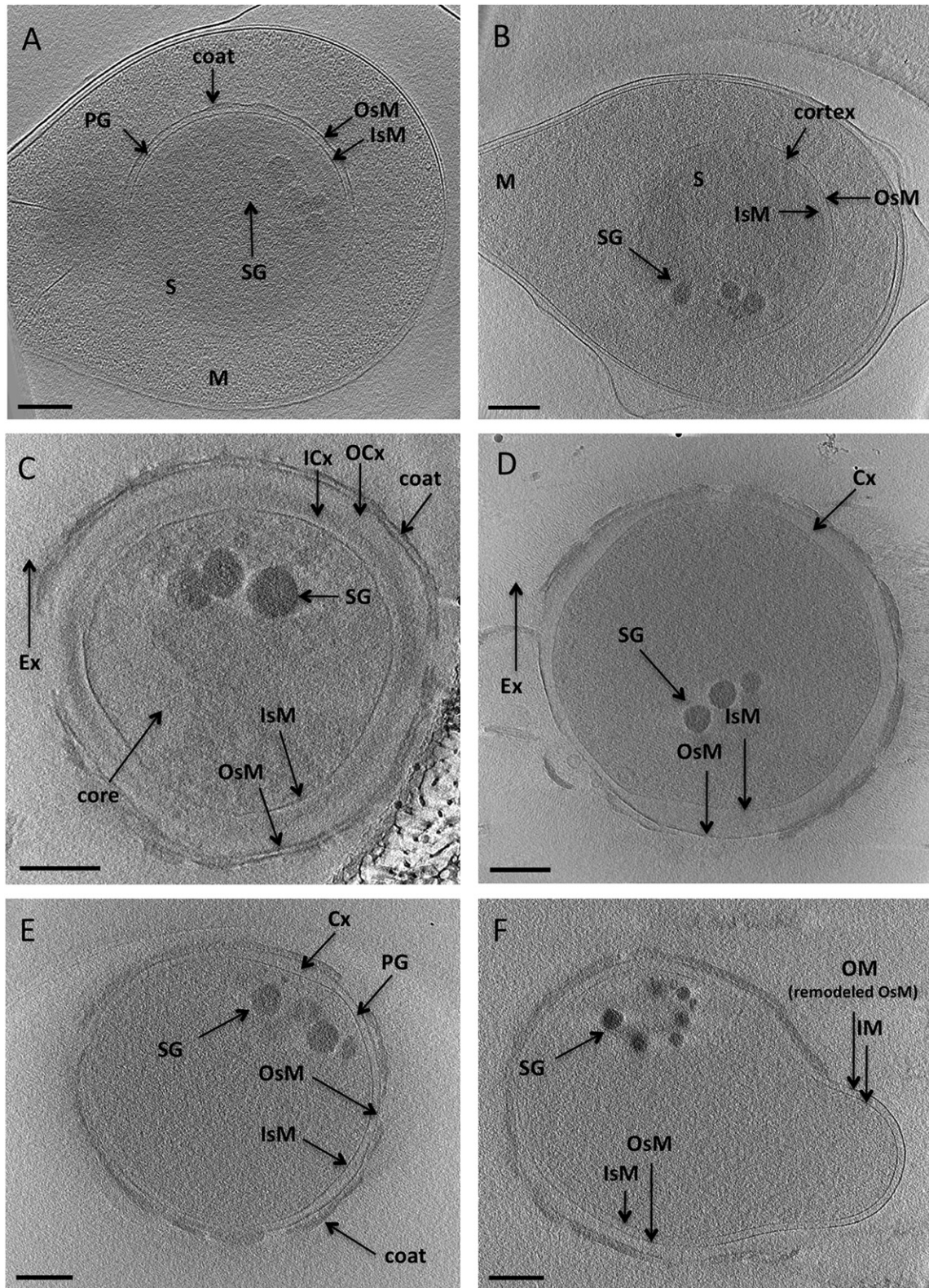


**Figure 2. Spore Maturation, Germination, and Outgrowth**

(A) A forespore (S) in the middle of a mother cell (M) is surrounded by a double membrane (IsM and OsM) and a PG layer between them. Multiple layers of coat are deposited on the outside of the OsM.

resulted in the formation of a forespore. While both membranes surrounding the forespore originated from the IM of the mother cell, we refer to these as the inner spore membrane (IsM) and the outer spore membrane (OsM) to distinguish them from the inner and outer membranes of the mother cell (Figure 1F). PG-like layers were observed between the IsM and OsM throughout engulfment.

### Spore Maturation

After engulfment and before the release of the mature spore via lysis of the mother cell, two layers of cortex between the IsM and OsM as well as coat layers outside the OsM of the forespore became apparent (Figures 2A and 2B). Due to the larger size of the sporulating cell and increased sensitivity to the electron beam, the reconstructions of the maturation process within the mother (five total) were lower quality. In Figure 2A the OsM nevertheless appears thicker and less regular, indicating the beginning of the coat formation. Figure 2B shows the beginning of cortex synthesis. In this cell, the space between the IsM and OsM had increased to ~40 nm and separate PG-like layers were no longer visible, suggesting the accumulation of cortex.

### Mature Spores

Due to the size and beam-sensitivity of mature spores, we augmented our studies of mature spores with traditional, room-temperature EM of plastic embedded thin-sections (Figure S2E). Two layers of cortex, labeled ICx and OCx, for “inner” and “outer” cortex, respectively, were apparent based on their differential staining with osmium tetroxide and uranyl acetate. The same two layers could also be seen in cryotomograms, though with smaller overall difference in contrast (Figure 2C). ECT of plunge-frozen *A. longum* spores revealed the continuing presence of the IsM and OsM as well as an exosporium (Ex) composed of tightly packed, hair-like structures ~200 nm in length and 2–4 nm in diameter (Figure 2D). From the inside out, the following distinct features were therefore discernable in a mature spore: core, SG, IsM, ICx, OCx, OsM, spore coat, and Ex. Notably, membranes, SGs and the Ex were not preserved by traditional EM methods, and may therefore have been less apparent in previous studies.

### Germination and Outgrowth

Pure spores (either heat-shocked or not) were placed in fresh 4YACo medium to induce germination and then plunge-frozen and imaged by ECT. No difference in the morphology between the heat-treated and untreated spores was observed, but since heat-shocked spores yielded faster-growing cultures, heat shock likely promoted germination. Spores at different stages of germination and outgrowth were present at each time point after induction, making it difficult to synchronize the cells or

determine the duration of germination. Vegetative cells were observed 12 hr after inoculation, however, indicating that the germination process can be completed within this amount of time. During germination, the cortex degraded nonuniformly (Figure 2D) until the distance between the IsM and OsM was again typical of a vegetative cell (~28 nm; Figure 2E and Figure S3C). Notably, where the OsM separated from the coat, the densities of the IsM and OsM appeared similar, suggesting that both membranes still had similar compositions (Figure S3C). Finally, the rupture of the protein coat of the spore accompanied outgrowth (Figure 2F). The area of the coat rupture where the new vegetative cell emerges has been termed “the cap” (Steichen et al., 2007). Multiple periplasmic layers were again discernable during outgrowth (Figure 3E and Figure S3D).

### The OM of *A. longum* Possesses LPS

Following the progression of the septa in the cryotomograms revealed that the OM of germinating cells was derived from an inverted section of the mother cell’s IM. Because the bacterial inner and OMs are so different in structure and function, the composition of *A. longum*’s OM was checked by several methods. First, whole cells of *A. longum* (and *B. subtilis* as negative control) were subjected to the Limulus Amebocyte Lysate test, a highly sensitive, FDA-approved test for LPS. While the *A. longum* sample contained LPS (126200 EU/ml), the *B. subtilis* sample did not (less than 0.5 EU/ml). Next, LPS was purified from *A. longum* (with *E. coli* BL21 and *B. subtilis* serving as positive and negative controls, respectively). An antibody raised against the lipid A portion of LPS from *E. coli* O157 cells and shown to recognize the LPS of other typical Gram-negative bacteria was used for western blots, which exhibited the hallmark ladder-like appearance of LPS (Chart et al., 1992) (Figure S4A). Pro-Q Emerald 300 stains confirmed the presence of the expected carbohydrate components of LPS (Figure S4B), controlling against the possibility of false positives from the antibody. Finally, the composition of *A. longum*’s LPS was investigated by GC-MS: after water:phenol extraction, in the water layer various glycosyl residues were found as well as several beta-hydroxy fatty acids, Kdo, and GlcN, all well-established hallmarks of LPS (Figures S4C and S4D).

With the presence of LPS in *A. longum* cultures firmly established, its location and time of appearance on the surface of outgrowing cells was investigated by immunofluorescence. While pure spores showed no immunofluorescence, immediately after outgrowth, the tip of the emerging cell fluoresced strongly (Figure 3F). Later stages of outgrowth also showed fluorescent signal from the outgrowing vegetative cell. Positive and negative *E. coli* BL21 and *B. subtilis* control cells behaved as expected (Figure S3).

(B) The IsM and OsM are separated apart (40 nm) as cortex is synthesized.

(C) The main features of a mature spore: core, storage granules (SG), IsM, inner and outer cortex (ICx, OCx, respectively), OsM, coat, exosporium (Ex; also see D).

(D) A germinating spore shows that cortex (Cx) hydrolysis is uneven. The IsM and OsM come closer together as the cortex gets degraded.

(E) Cortex degradation nears completion before outgrowth begins.

(F) Outgrowth of a bacterium shows the new IM and OM that are derived from an IsM and the OsM. Again each panel is a 20 nm thick tomographic slice through a 3D reconstruction.

Scale bars represent 200 nm. See also Figure S2.

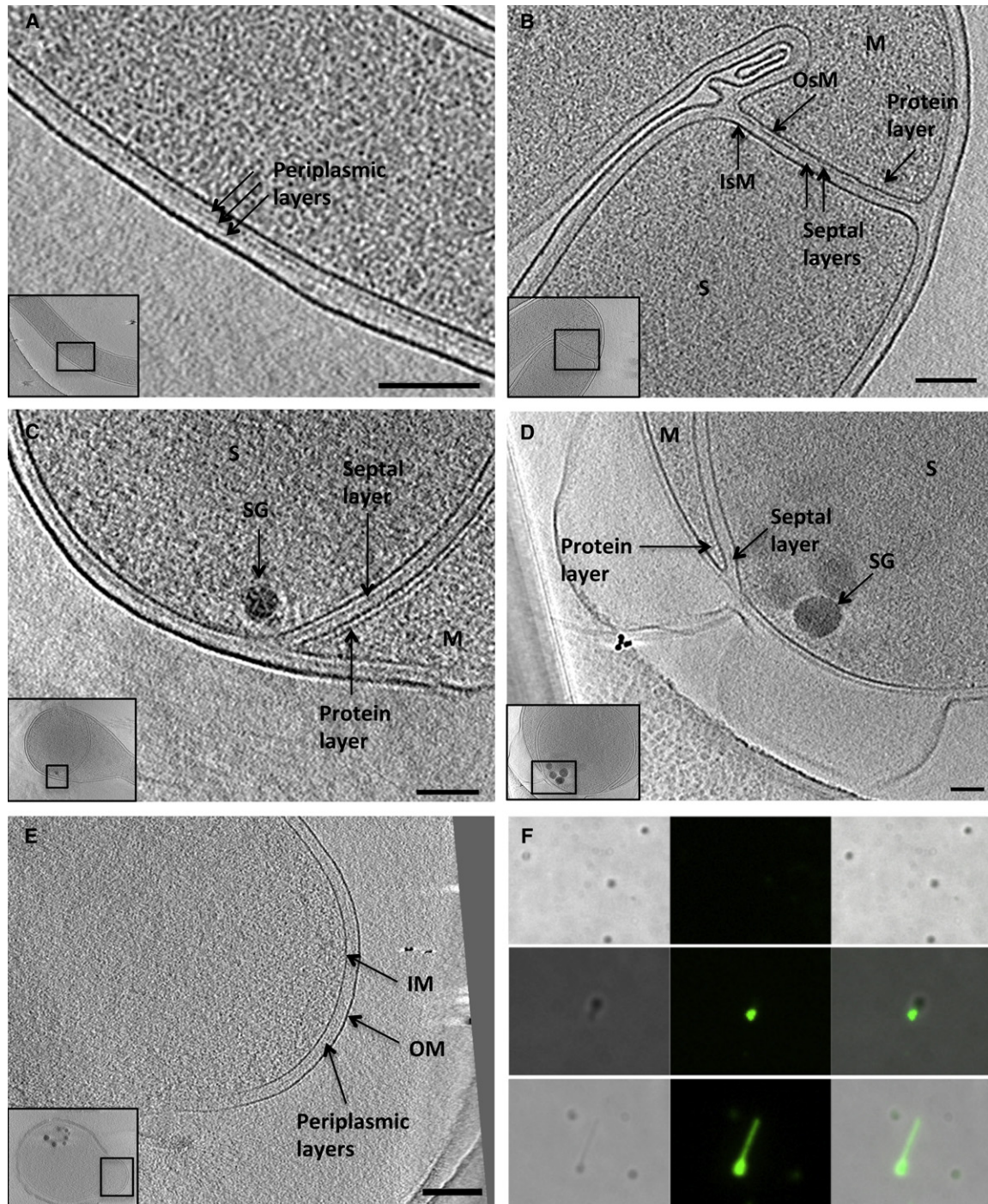


**Figure 3. Structural Details**

(A) Two to three periplasmic layers are observed between the IM and OM of vegetative cells.

(B) Septa at early stages of sporulation exhibit two septal layers of density between the IsM and OsM. The layers are continuous with the innermost periplasmic layer. A layer of protein density is observed on the mother side of the septum.

(C) Leading edge of an engulfing membrane. A layer of septal material is present between the IsM and OsM, a protein layer is connected to the mother side of a septum and appears as regularly spaced densities connected to the OsM, and storage granules appear at the leading edge of the engulfing membranes.

(D) Advanced stage of engulfment. The number and size of the SG increases, the septal layer between the IsM and OsM is still observed, a protein layer is also present on the mother side of OsM.

(E) Presence of periplasmic layers between the IM and the OM of an outgrowing cell.

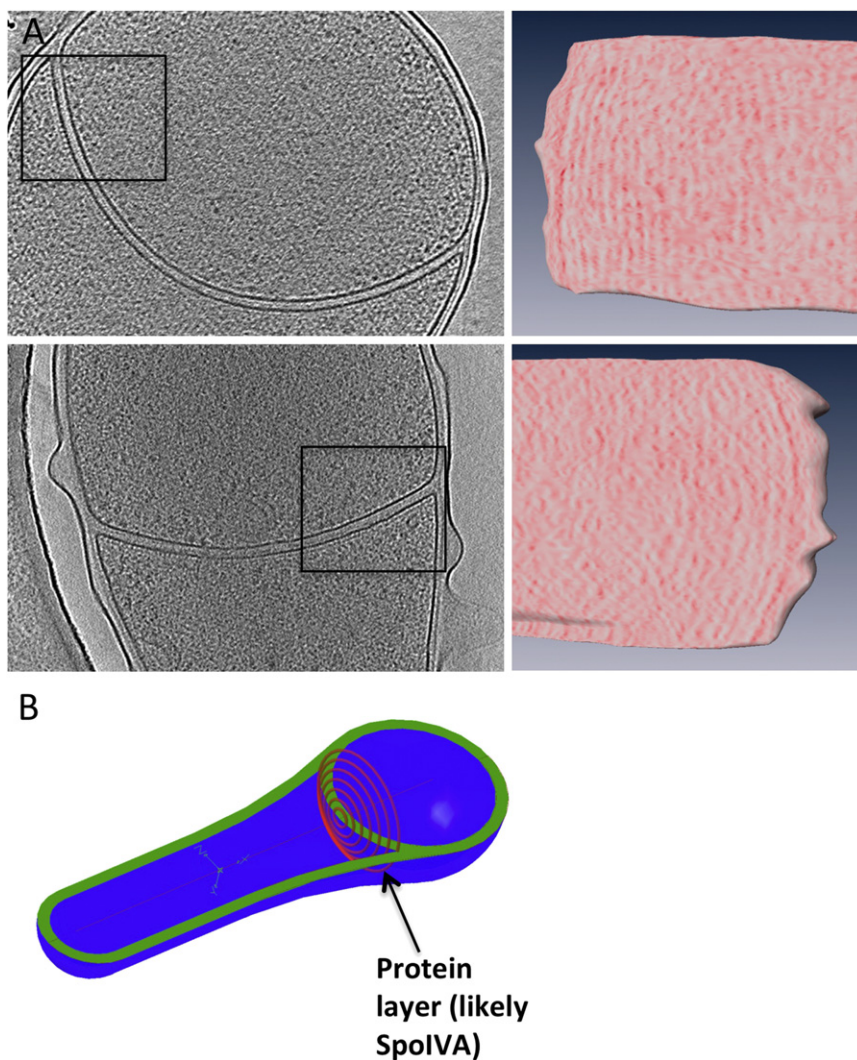


**Figure 4. Higher Order Structure of a Protein Layer on the Mother Side of the Septum**

(A) Density projections of a protein layer on the mother side of the OsM. Left: Tomographic slices through the cells showing the shape of the OsM and the protein density connected to it. Right: Projection of all the density within 5–15 nm on the mother cell's side of the OsM, revealing concentric, parallel cables. Control projections of density both further into the mother cell and on the spore side of the IsM appear random (data not shown). (B) Schematic representation of the pattern generated by the observed protein layer (red rings) on the mother side of the OsM.

pendicular to the beam difficult to discern, this pattern means that the cables form either concentric rings or a spiral (Figure 4B).

#### Negative-Staining and ECT Studies of Purified Sacculi

As described above, PG-like layers were present within the periplasm of vegetative cells, within septa throughout engulfment, and within the forespore between the IsM and OsM (Figure 3). To test whether the septal layers contained PG, sacculi of *A. longum* cells at different stages of engulfment were purified and imaged. While sacculi of vegetative cells were rod shaped, sacculi from sporulating cells were easily recognized by their enlarged poles. Negative staining of the purified sacculi showed round, approximately semi-circular dark patches near the tip of the enlarged pole consistent with the pattern that would be expected

#### Protein Layer Coating the OsMs

A layer of ordered protein density was present on the outside of the engulfing OsM of sporulating cells (Figures 3B–3D). The densities appeared equally spaced, were  $\sim 2.4$  nm wide, and showed clear connectivity to the OsM. Since this layer appeared right after septum formation and was present throughout engulfment, we believe that one of the components of the protein layer is likely SpoIVA (Ramamurthi et al., 2006). This protein layer was clearly visible in a density profile of the septum (Figure S3B) and was located  $\sim 12$  nm (peak to peak) from the OsM. By projecting this layer of density onto the OsM, the layer was seen to be organized as a series of parallel, concentric cables (Figure 4A). Accounting for the well-understood effects of the “missing wedge” in tomography, which elongates all densities along the direction of the electron beam and makes lines per-

for collapsed prespores surrounded by the peptidoglycan of the mother cell (Figure 5A and Figure S5). Other sacculi exhibited very dark, spherical, spore-like shapes near the center of the enlarged pole suggesting that once the spore cortex matures, spore contents were trapped inside despite the harsh preparative procedure (Figure S5F). All imaged mother cell sacculi contained extra densities suggestive of prespore, forespore, or mature sacculus PG layers inside, but folds in the collapsed sacculi collected stain and complicated detailed interpretation.

Purified sacculi were therefore also imaged with ECT (Figure 5B and Figure S6). In cryotomograms the cell wall surrounding sporulating poles was noticeably thicker than the wall surrounding vegetative cells. Numerous granules were observed within the sacculi of sporulating but not vegetative cells. These are likely glycogen, since energy storage is expected

(F) Immunofluorescence images of quiescent (top) and outgrowing spores (middle and bottom) showing that LPS appears on the surface of *A. longum* cells immediately upon outgrowth.

Insets show the area of a cell that has been magnified. Scale bars represent 200 nm. See also Figures S3 and S4.

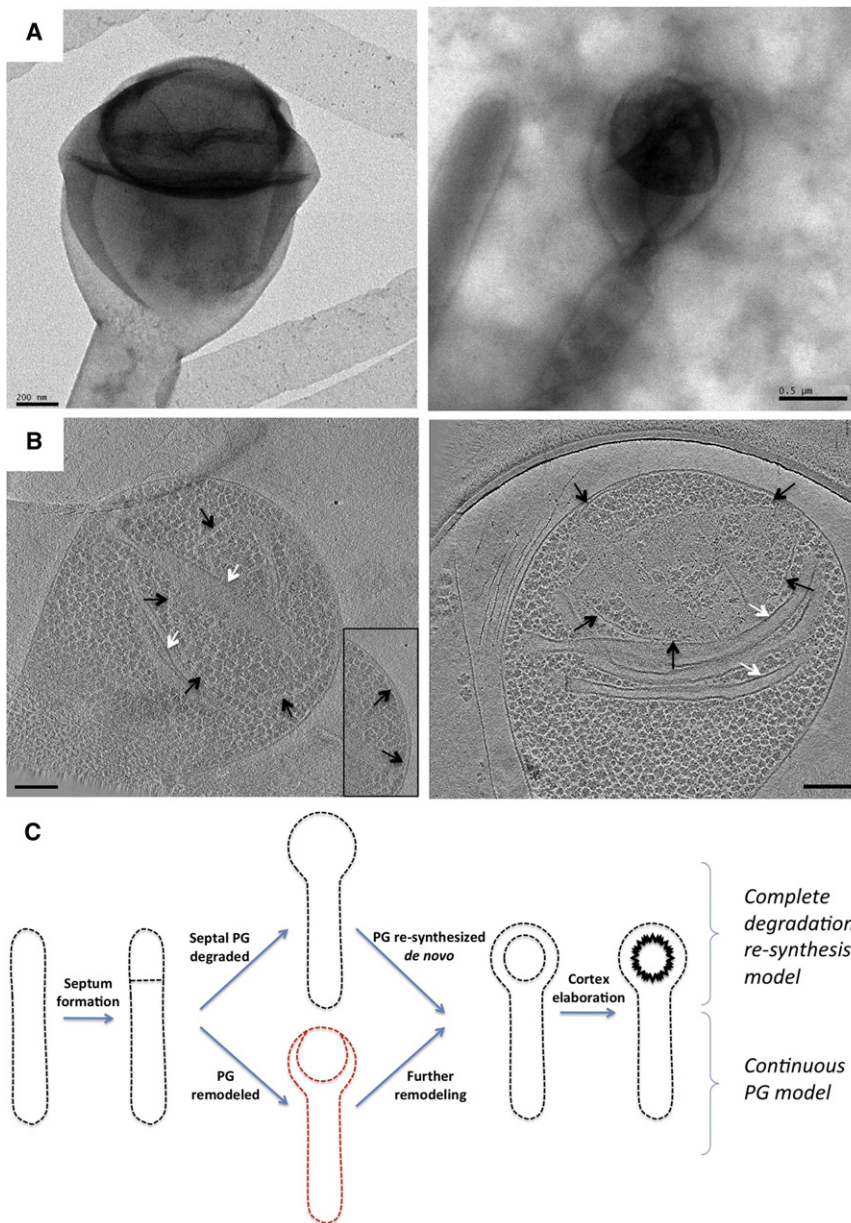


**Figure 5. Peptidoglycan Is Present between the IsM and OsM during Engulfment**

(A) Images of negatively stained, collapsed sacculi of engulfing cells.

(B) Tomographic slices through reconstructions of purified sacculi of engulfing cells. Black arrows mark the prespore PG and white arrows mark folds in the mother cell PG caused by the collapse of the sacculi on the EM grid. The inset shows a slice where the prespore PG can be seen merging with the mother cell PG at the tip.

(C) Two models for the structure and role of PG during sporulation. The key difference is the presence of PG between the IsM and OsM during engulfment, as highlighted in the red intermediate unique to the “continuous PG” model.

Scale bars represent 200 nm. See also Figures S5 and S6.

extreme tip of the mother cell. In some cases the boundary of the sack could be seen merging with the thicker mother cell wall around the tip, as would be expected of an engulfing septal PG. Numerous small, high-contrast (black) spherical densities were also observed scattered over the region enclosed by and along the boundary of the sacks, as if they were specifically bound to the collapsed sack material, fortuitously marking its extent amidst the folds. We conclude that engulfing prespores are surrounded by PG.

### Genome Analysis

The genome of *A. longum* was sequenced with a 454 Flex Pyrosequencing platform. Based on SSU rRNA analysis *A. longum* belongs to the bacterial phylum *Firmicutes* (Kane and Breznak, 1991). Within this phylum, *A. longum* groups with the *Veillonellaceae*, a phylogenetically coherent family within the class *Clostridia* (Figure 6) (Rainey, 2009).

during sporulation and the purification procedure involved proteases, nucleases, harsh denaturants and detergents (boiling SDS) that would have destroyed other noncarbohydrate cellular macromolecules. While the granules were densely packed within the collapsed sacculi, they would not have been so in the inflated, living state. Prominent folds in the mother cell wall exhibited a characteristic pattern of two thick walls on either side of a cleft bereft of granules. Fully engulfed spores were easily identified due to their high contrast, size (known well from cryotomography of intact cells), and random placement within the enlarged pole of the mother cell. In addition to the folds, granules, and forespores, however, a thinner, vegetative-PG-like sack could be seen. The shape and size of the sacks matched those of engulfing prespores and the sacks were always found at the

To investigate how the seldomly combined sporulation and Gram-negative phenotypes could have arisen in *A. longum*, we compared *A. longum*'s genome to those of other bacteria. First, using phylogenetic profiling (see the [Extended Experimental Procedures](#)), we ranked the Pfam domains most strongly associated with the classification “Gram negative,” and then, separately, with the ability to form endospores (from 1080 and 769 completed genomes, respectively). As expected, the genes most strongly correlated with Gram-negativity coded for known OM proteins such as LpxB-D and K, TolC, and Omp85. Components of the flagellar motor that localize to the OM (FlgH and FlgI) also scored highly (in the top 45, data not shown). Again not surprisingly, the genes that correlated most strongly with endospore formation included SpoIVA, SpoIIAE, SpoIIP,

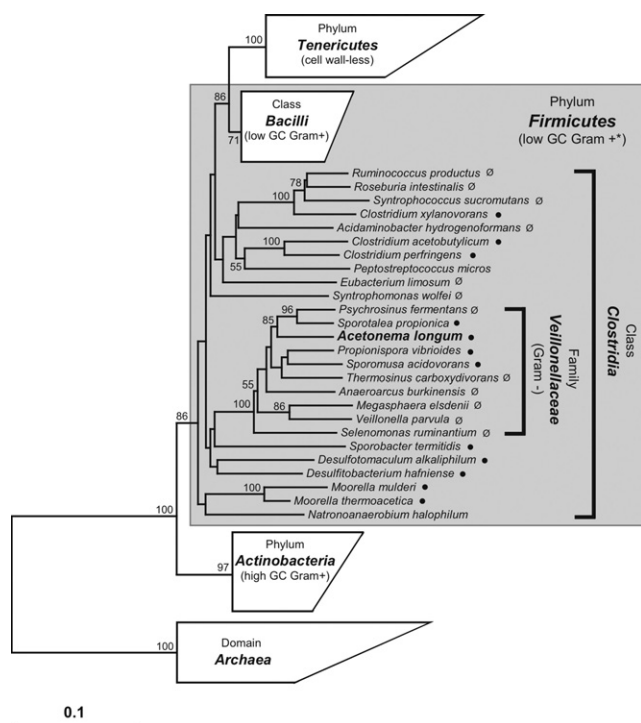


**Figure 6. SSU rRNA Phylogenetic Tree**

The tree was constructed using the Fitch Distance method with Kimura 2-parameter correction and was based on 1117 unambiguously aligned nucleotide positions. The *A. longum* 16S gene sequence was aligned to the database, which incorporated the Silva SSU alignment (<http://www.arb-silva.de>), using parsimony methods. Values at nodes represent percent support for 1000 step bootstrap parsimony analyses of the dataset. Bar represents 10% sequence variation. Symbols: ●, documented sporulation, ○ sporulation not observed. Where no symbol is given, spore formation was not classified. ★ Certain members of the phylum Firmicutes are classified as Gram-negative or Gram-variable. See also Figure S7 and Table S2.

and YabG. Homologs of nearly all the genes near the top of both lists were found in *A. longum* (Table S2). Thus, *A. longum* possesses a typical OM with proteins homologous to those found in numerous other Gram-negatives and forms endospores with the same basic machinery as other Firmicutes. These facts argue against either phenotype arising from convergent evolution.

To investigate whether either phenotype was likely the result of a recent horizontal gene transfer across phyla, we calculated phylogenetic trees for Omp85, TolC, LpxB-D, SecY, FlgH, and FlgI, which are associated with Gram negativity, and SpoIVA, SpoIIP, SpoVB, and SpoIIIAE, which are predictive of endospore formation. One example of each (Omp85 and SpoIVA) is shown in Figure S7. The Omp85 protein family tree grouped *A. longum* with other members of Veillonellaceae but showed no clustering to any particular class of Gram-negative bacteria (Figure S7A). In contrast, the evolutionary relationship of chloroplasts to cyanobacteria and mitochondria to  $\alpha$ -proteobacteria was clear. The SpoIVA family tree revealed *A. longum* and *Thermosinus carboxydivorans*, another member of the family Veillonellaceae, as a deeply branching and robustly-supported clade within

the Clostridia class, separate from the Bacilli (Figure S7B), as expected from SSU rRNA-based species phylogeny. The trees for the other genes analyzed gave similar results, arguing against recent horizontal gene transfers as the source of either phenotype.

## DISCUSSION

This study reports a comprehensive imaging survey of the processes of sporulation and germination in *A. longum*. We imaged a Gram-negative sporulating bacterium; the cells were preserved in a near-native, “frozen-hydrated” state free from fixation, dehydration, and staining artifacts; and the cells were imaged tomographically, resulting in full 3D reconstructions. As a result, details about periplasmic and septal layers, storage granules, protein coats, and membranes were obtained suggesting models for the role of PG in sporulation and the evolution of the OM in bacteria.

### Protein Localization on the Mother Side of the Engulfing Membranes

We observed a layer of concentric rings (Figure 4A) on the mother side of the septum throughout engulfment (Figures 3B–3D) that was clearly connected to the OsM. A candidate for the observed density is SpoIVA, an ATPase that is synthesized under the control of  $\sigma^E$  and appears immediately after septation (Roels et al., 1992; Stevens et al., 1992). In vitro, SpoIVA irreversibly self-assembles into bundles of cables  $\sim 10$  nm in diameter (Ramamurthi and Losick, 2008). SpoIVA has been shown to be the base layer for attachment of more than 50 other coat proteins to the outer surface of the maturing spore after engulfment is completed, starting with CotE and CotJ (Driks, 2002). The predicted globular diameter (2.4 nm) (Erickson, 2009) and the width of the observed densities in our tomograms ( $\sim 2.5$  nm), supports the notion that the regularly spaced cables in *A. longum* correspond to SpoIVA, and we found a clear homolog of SpoIVA in the genomic sequence of *A. longum* (55% sequence identity to the protein in *B. subtilis*). Thus, we believe SpoIVA polymerizes into densely packed, concentric rings as engulfing membranes propagate around the prespore, exposing additional surface at the periphery (Figure 4B).

Ramamurthi et al. recently proposed a mechanism for how SpoIVA is localized to the septum in *B. subtilis*. A 26 amino acid protein, SpoVM, forms an amphipathic helix that adheres to convex membranes via hydrophobic interactions (Ramamurthi and Losick, 2009). Affinity chromatography experiments showed that SpoIVA binds to SpoVM, suggesting that SpoVM targets SpoIVA to the curved engulfing membranes on the mother side of a septum. The literature has been ambiguous, however, about whether homologs of SpoVM exist in Clostridia (Onyewoke et al., 2004; Prajapati et al., 2000). We searched for homologs in all sequenced Clostridia and many other sporulating species. Endospore-formers outside the family Veillonellaceae that possessed *spoIVA* also had a homologous sequence for *spoVM*, but surprisingly, the only two members of the family Veillonellaceae that have been sequenced and shown to sporulate (*T. carboxydivorans* and *A. longum*) lacked *spoVM* but had *spoIVA*. While it is possible that the sequencing coverage was

incomplete, another possibility is that a different protein or mechanism serves the role of SpoVM in *Veillonellaceae*. We favor this idea because the putative SpoIVA protein layer we saw on the mother side of a septum localized there even before the septum began curving (Figure 3B), an observation quite different from *B. subtilis* (Ramamurthi et al., 2009).

### Peptidoglycan and Cortex

Because *A. longum* possesses both an inner and an OM throughout sporulation and germination, the data presented here call attention to the continuity and development of the PG and cortex structures that fill the intermembrane space. PG is required for septation (Yanouri et al., 1993), and previous EM studies have shown PG is present in the septum right after septation (Hilbert and Piggot, 2004), but the fate of the septal PG thereafter is an active area of research. Thin-section EM images of sporulating *Bacilli* exhibit septa that are thinner and more irregular than the external cell wall, calling into question whether PG is retained (Gueiros-Filho, 2007). Numerous studies have reported that PG in the septum is completely degraded, starting at the center of the septum where closure occurs (Errington, 2003; Smith et al., 2000). PG hydrolase activity has been detected during engulfment and mutants that lack key PG hydrolases fail to complete engulfment (Errington, 1993; Illing and Errington, 1991). The formation of the SpoIIQ - SpoIIAH channel between the mother and the forespore was suggested to depend on the lack of PG between the septum membranes (Blaylock et al., 2004), and SpoIIIB was identified as the PG hydrolase necessary for degrading PG (Perez et al., 2000). PG hydrolysis was also shown to persist throughout membrane migration (Gutierrez et al., 2010). After engulfment, two new layers of material were described between the IsM and OsM (Doi, 1989), and the synthesis of these new layers was defined as “stage IV” of sporulation (Buchanan et al., 1994). Based on the compositions of the two layers, it was suggested that one gives rise to the spore cortex, which is later discarded in germination, while the other persists to become the future vegetative cell wall (Henriques and Moran, 2007; Tipper and Linnett, 1976). Taken together, the model that emerges from the existing literature is therefore one of “complete degradation/resynthesis,” in which PG is used to advance the septum, but then is completely degraded, only to be re-synthesized later de novo as a double-layered foundation for the cortex and the future vegetative cell wall (Figure 5C).

PG-like densities were observed by cryotomography here, however, in the vegetative cell wall, within septa, between the IsM and OsM, in the cortex of mature spores, and during outgrowth. A key issue is whether these layers, and in particular the septal layers, are PG, or alternatively, if one or more are simply proteinaceous, consisting of for instance the periplasmic domains of integral membrane proteins or other proteins closely associated with a membrane. To test this, we purified sacculi from sporulating cells. The procedure involves treatments with detergents, nucleases, proteases, and boiling denaturants to remove all other cellular components besides large carbohydrate superstructures like glycogen granules and PG. If PG persists in septa throughout sporulation, engulfing sacculi should exhibit internal prespore compartments ranging from

nascent septa to partially closed hemispheres (Figure 5C). With traditional EM and cryotomography methods, we observed many sacculi from engulfing cells that contained an additional internal “sack” fully consistent in size, shape, and position with prespores (Figure 5 and Figures S5 and S6). Thus, our results support a much simpler, “continuous PG” model in which the peptidoglycan required for septum formation is not completely hydrolyzed (Figure 5C). Instead, the PG produced during septation is remodeled during engulfment, then elaborated to form the two layers of cortex during spore maturation, and finally restored to its original (thin) state during germination to become the cell wall of the vegetative PG (Figure 3E). This model obviates the need to construct PG layers de novo (either the cortex or later the outgrowing cell wall), a process without known precedent (Joseleau-Petit et al., 2007).

It seems reasonable that the cortex in pure spores could be derived from the septal PG because the structure of cortical PG is similar to vegetative PG, though less crosslinked (Atrih et al., 1996; Popham et al., 1996). The two septal PG layers likely serve as the foundation of the two cortices, which are simply expanded with modified building blocks. PG remodeling would require hydrolases such as SpoIIIB and SpoIIID, as described above, but also PG synthases to either drive or at least accommodate the morphological changes. Two promising candidate PG synthetases are MurG and MurAA, whose inhibition by fosfomycin blocked engulfing membrane migration (Meyer et al., 2010). Homologs of MurG and MurAA are present in *A. longum*.

Once the environment becomes favorable, spores germinate. For this to occur, nutrient molecules have to bind to receptors located on the IsM (Setlow, 2008). The first triggered event upon germination initiation is the release of dipicolinic acid and calcium ions from the spore coat and their replacement by water. Previous studies on *Bacillus anthracis* suggested that the release of these molecules also stimulated cortex hydrolases (such as YaaH [Dowd et al., 2008]), which in our model would be needed to degrade the thick layers of cortex between the inner and outer forespore membranes. A molecular determinant that governs the hydrolysis of the cortex material but not the vegetative PG during germination could be the difference in composition and cross-linking between the two. At the end of cortex degradation in *A. longum*, we observed the thinning of the two cortex layers into what became the multiple periplasmic layers in vegetative cells (Figure 2F and Figure S3D), supporting the notion that both are PG.

The continuous PG model has an intriguing implication. It suggests that *A. longum* can expand a thin, “Gram-negative” PG layer into a thick cortical layer that in other *Firmicutes* becomes the Gram-positive cell wall, and then reverse the process in germination. This suggests that Gram-negative and -positive cell walls share a common foundation and basic architecture. By direct imaging, we recently showed that the Gram-negative PG wall is “layered” (Gan et al., 2008), so Gram-positive walls are probably layered too (for other possibilities, see Dmitriev et al., 2003; Hayhurst et al., 2008).

### Transformation of an IM into an OM

As with *Bacillus* and *Clostridium* spp., the sporulation septum in *A. longum* was generated by invagination of the IM (Figure 1B).

This septum formed the two membranes (the IsM and the OsM) that surrounded the immature spore and that were visible throughout engulfment (Figures 1B–1F). Even though the IsM and OsM were not observed in the plastic-embedded sections of pure spores (Figure S2E) (Henriques and Moran, 2007), they were discernable in the cryotomograms (Figures 2B–2E). The inner and outer cortex layers were deposited between the inner and OsMs. The OsM was clearly visible during coat hydrolysis and then outgrowth (Figures 2E and 2F), when it emerged as the OM of the germinating cell (Figure 7, Movie S2, Movie S3).

The presence or absence of an OsM during spore maturation and germination has not been discussed previously, since the other members of *Bacilli* and *Clostridia* that have been studied possess only a cytoplasmic membrane and therefore lose their OsM during outgrowth. As a simple result of the topology of engulfment, however, two membranes surround the mature endospores of all sporulating bacteria. Thus, a common morphological state exists between all double- and single-membraned sporulating bacteria. *A. longum* retains its second membrane during germination whereas other endospore-forming *Bacilli* and *Clostridia* lose theirs. Intriguingly, then, our data show that *A. longum*'s OM is derived from an “inverted” IM of the mother cell.

OMs are typically very different, however, from IMs in protein composition, the presence of lipopolysaccharide, and permeability. Yet, by all indications, *A. longum*'s second membrane is a bona fide, fully differentiated OM that is part of a typical Gram-negative bacterial cell envelope: (1) *A. longum* fails to retain the Gram stain just like all other typical Gram-negative cells (data not shown); (2) the OM of *A. longum* appears just slightly denser in cryotomograms than the IM (Figures 3A–3C and Figure S3A), just as has been observed in other Gram-negative bacteria (Briegel et al., 2009), confirming its special composition and structure; (3) the entire envelope, including the width of the periplasm, the appearance of the peptidoglycan layers, and the presence of flagella spanning both membranes with accompanying rings are all typical of Gram-negative bacteria; (4) *A. longum* produces LPS, as confirmed here by western blotting, Pro-Q Emerald 300 staining, the LAL test, and gas chromatography-mass spectrometry (Figure S4) (Kane and Breznak, 1991); (5) the LPS appears on the surface of cells immediately upon outgrowth, as shown here through immunofluorescence (Figure 3F and Figure S3A); and finally (6) 22 of the top 25 Pfam domains that correlate most strongly with Gram-negativity are present in *A. longum* including OM proteins (Omp85, TolC), flagellar proteins (FigH, FigI), periplasmic chaperones (Skp), and LPS biosynthesis proteins (LpxA-C, MsbA) (Table S2, part A). (Ironically, the term “OM” was actually *first* applied to a member of the *Veillonellaceae* [Bladen and Mergenhagen, 1964], and only later was the term widely accepted and used to describe the structure in all other Gram negatives!)

The IM of sporulating *A. longum* cells must therefore be transformed in composition and function during sporulation, germination, and outgrowth into a typical OM. We do not know exactly when this transformation occurs, but based on our immunofluorescent experiments (Figure 3F) and density profiles of membranes at different stages of sporulation (Figure S3), we hypothesize that LPS is synthesized when the outgrowing cell

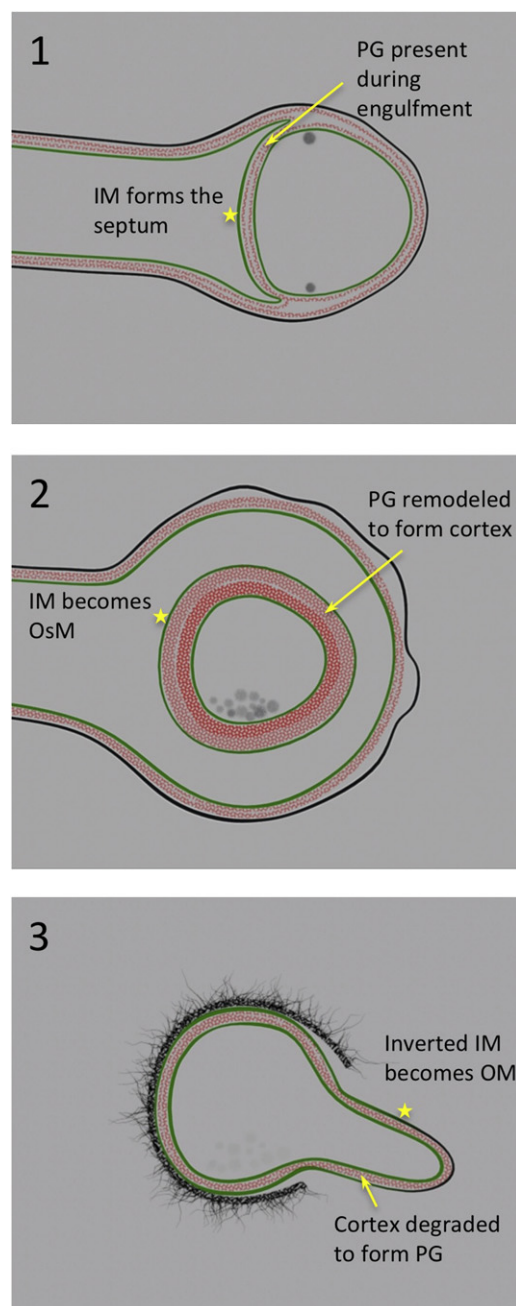


**Figure 7. Schematic Highlighting Key Findings**

Frames 1–3 were taken from Movie S2 and illustrate the transformation of an IM (IM, green) to an OsM (green) and finally the OM (black) of an outgrowing cell. A yellow star is used to show that the IM also gets inverted in the process. PG is shown in red and is present in the septum throughout engulfment, elaborating to form the cortex of the mature spore and then degrading to restore the thin cell wall of the outgrowing cell. See also Movie S2 and Movie S3.

begins to elongate out of the spore. As the OM grows, new material including LPS and beta-barrel porins is likely added. This then simply dilutes out the initial IM material.

### Evolutionary Implications

How the OM first arose in Bacteria is an interesting question (Cavalier-Smith, 2004). It has been suggested that a symbiosis between an ancient actinobacterium and an ancient clostridium produced the last common ancestor of all double-membraned bacteria (Lake, 2009). Over long periods of time, some or all of the outer genome could have transferred into the inner organism. An alternative hypothesis is that a single-membraned cell autogenously evolved the machinery to synthesize a second membrane. One could imagine an internal vesicle being repurposed to serve as an IM, and the genome being moved to within the vesicle, or alternatively that external patches of membrane arose and then expanded over generations (proteins are known which could stabilize unclosed patches of membrane). If it were ever found that spheroplasts (Gram-negative bacterial cells stripped of their OM) could recover their OMs by extruding OM material, this would constitute strong support for this hypothesis.

Our work with *A. longum* reveals a third possible mechanism, however, and shows that it does in fact happen in nature frequently (every time *A. longum* germinates): second membranes are generated by sporulation and can then be transformed into typical LPS-containing OMs. Considering a primordial single-membraned cell with the capability to form a septum and divide, a small number of mutations might be required to cause the membrane of one daughter cell to stick to the other, which might eventually lead to some kind of engulfment and primitive sporulation. The single genome directing this process would already be found inside the spore. If upon escape from the engulfing mother cell (some kind of primitive “germination”), the second membrane were retained, as it is in *A. longum*, a double-membraned vegetative cell would emerge. Over generations the OM could have evolved to have very different properties than the IM. Whether or not this is the mechanism by which all OMs in Bacteria arose we may never know, but *A. longum* makes it clear that the basic membrane transformations can and do happen.

One test of this hypothesis (that a primitive sporulation-like process gave rise to the bacterial OM) is whether *A. longum*'s abilities to elaborate an OM and sporulate are ancient and widely shared, or alternatively are the result of either recent horizontal gene transfers or convergent evolution. To explore these questions, we used phylogenetic profiling to objectively rank genes that are most predictive of an organism's ability to either sporulate or form an OM, and then created phylogenetic trees of several top-scoring genes (Figure S7). In each of the proteins we analyzed (Omp85, TolC, LpxB-D, SecY, FlgH, and FlgI, for OM), *A. longum* grouped with *Thermosinus carboxydivorans*, another member of the *Veillonellaceae* family, but not with any other Gram-negative bacteria outside the *Veillonellaceae* (Figure S7A). Thus, there is no evidence to suggest that recent lateral gene transfer played a role in its acquisition of an OM. The possibility of convergent evolution of the OM in the *Veillonellaceae* is ruled out by the presence of many unambiguous homologs of different subsystems associated with OM biogenesis and function in other Gram-negative phyla. Concerning sporulation, phylogenetic trees of *Firmicute* sporulation genes showed the same basic evolutionary relationships as their 16S ribosomal subunit (Figure S7B), again arguing against any recent horizontal

gene transfer or convergent evolution. *A. longum*'s machinery to form an OM and sporulate therefore derives from *widely shared, ancient* sources, supporting our hypothesis that the origin of the OM in all Bacteria could have been a primitive sporulation.

Finally, our studies of *A. longum* shed light on the evolution of the *Firmicute* phylum itself. Since all endospores pass through a common state with two membranes, we speculate that the last common *Firmicute* ancestor was also double-membraned. The diversity of the *Firmicutes* and the associated phylum *Tenericutes* could then be explained by losses of OM and/or sporulation properties rather than separate evolutionary gains: some members of the family *Veillonellaceae*, including *A. longum*, retained both properties while others (such as *Selenomonas ruminantium*) lost the ability to sporulate but retained an OM. Conversely, many of the *Clostridia* and *Bacilli* retained their ability to form endospores but lost their OM, perhaps for reasons of increased sporulation and germination efficiency. Others (such as *Ruminococcus productus*) lost both the ability to sporulate and their OM, as did the *Tenericutes*, which further discarded PG.

Loss of entire gene suites is plausible, since it is now known, for instance, that there are very few pseudogenes in bacteria, as these are removed right away (Kuo and Ochman, 2010), and that mitochondria have lost nearly all of their genes. It is certainly easier to imagine unneeded genes being lost from bacterial lineages than gained, since acquisition requires that they be integrated into the existing networks in a fashion that immediately enhances (or at least preserves) cellular fitness. It is important to note, however, that our hypothesis does not require that modern *Firmicutes* be ancestral to any or all of the Gram-negatives. We are only proposing that a single-membraned last common ancestor of both *Firmicutes* and Gram-negatives possessed some primitive sporulation/phagocytotic-like ability, which gave rise to the OM. From this double-membraned sporulation ancestor many phyla could have diverged. Any one of these could have lost the OM and given rise to the *Firmicutes*. Other phyla could have lost the ability to sporulate at different times, giving rise to the current models of microbial phylogeny.

### EXPERIMENTAL PROCEDURES

#### Sample Preparation

Vegetative *A. longum* strain APO-1 (DSM 6540) and sporulating cells were grown anaerobically as described (Leadbetter and Breznak, 1996). For ECT studies on sporulation, cells were harvested from cultures entering stationary phase. At this time, phase-bright (mature) spores were clearly visible and were still contained within mother cells. Pure spores were harvested by centrifugation and purified from mother cells as described (Nicholson and Setlow, 1990). For ECT studies on germination, purified spores were added to growth medium and either heat-shocked or not. Images of cells harvested 6, 7, 8, and 9 days after inoculation and spores harvested 0 hr, 4 hr, 8 hr, 12 hr, and 24 hr after inoculation were collected. Sacculi were prepared as described (Poindexter and Hagenzieker, 1981). Samples were plunge-frozen across EM grids as described (Iancu et al., 2006).

#### EM Data Collection and Processing

Cryotomograms of vegetative (~200), sporulating (~150) and germinating (~50) *A. longum* cells and mature spores (~50) were collected with an FEI Polara (FEI Company, Hillsboro, OR) 300 kV FEG transmission electron

microscope equipped with a Gatan energy filter and a lens-coupled 4k × 4k UltraCam (Gatan, Pleasanton, CA). Three-dimensional reconstructions were calculated with IMOD (Kremer et al., 1996) and analyzed with Amira (Mercury Computer systems) and in-house software. Purified sacculi were dried on glow-discharged EM grids, stained with 1% uranyl acetate, and imaged with a Tecnai T12 EM. Chemical fixation of pure spores was based on protocols developed by Sabatini et al. (Sabatini et al., 1963).

#### Immunofluorescence

Germinating spores were fixed, washed, deposited onto glass slides, air-dried, blocked, and incubated with primary and then secondary antibodies. The primary antibody used in this study was a polyclonal goat Ab raised against the lipid A portion of LPS from *E. coli* O157. See the [Extended Experimental Procedures](#) for more details.

#### Phylogenetic Analysis

Genomic DNA was sequenced with a 454 Flex Pyrosequencing platform. Protein phylogenies were constructed using the MUSCLE algorithm (Edgar, 2004). Protein trees were constructed with PHYLIP. Values given above the nodes of trees represent percent support calculated with 100 bootstrap maximum likelihood analyses of the datasets. Nodes indicated with dots are confirmed and supported by 100 bootstrap protein parsimony analyses.

#### ACCESSION NUMBERS

The *Acetonebma longum* DSM 6540 accession number of the genomic sequence reported in this paper is AFGF01000000.

#### SUPPLEMENTAL INFORMATION

Supplemental Information includes Extended Experimental Procedures, seven figures, two tables, and three movies and can be found with this article online at [doi:10.1016/j.cell.2011.07.029](https://doi.org/10.1016/j.cell.2011.07.029).

#### ACKNOWLEDGMENTS

We thank Alasdair McDowall and Mark Ladinsky for their help with the preparation of mature spores by traditional EM methods and Dr. Martin Pilhofer for helping with the immunofluorescence and western blotting experiments. The GC-MS analysis of LPS was performed at the Complex Carbohydrate Research Center and was supported by DOE grant DE-FG02-09ER20097. We thank Everett Kane for the generation of [Movie S2](#) and Jane H. Ding for helping with the generation of [Movie S1](#) and [Movie S2](#). We thank Ivan Tochev for generating [Figure 4B](#). We thank Dr. Stephen Quake and Richard White at Stanford University for performing the shotgun genome sequencing of *A. longum*. The authors gratefully acknowledge the IGS annotation engine. This work was supported by a Natural Sciences and Engineering Research Council of Canada Postdoctorate Fellowship (to E.I.T.), the Howard Hughes Medical Foundation, and gifts to Caltech from the Gordon and Betty Moore Foundation, including support for the Caltech Center for Integrative Study of Cell Regulation. E.G.M was supported by the Department of Energy (award DE-FG02-07ER64484 to J.R.L.).

Received: November 2, 2010

Revised: May 25, 2011

Accepted: July 9, 2011

Published: September 1, 2011

#### REFERENCES

Atrih, A., Zöllner, P., Allmaier, G., and Foster, S.J. (1996). Structural analysis of *Bacillus subtilis* 168 endospore peptidoglycan and its role during differentiation. *J. Bacteriol.* **178**, 6173–6183.

Bechtel, D.B., and Bulla, L.A., Jr. (1976). Electron microscope study of sporulation and parasporal crystal formation in *Bacillus thuringiensis*. *J. Bacteriol.* **127**, 1472–1481.

Ben-Harush, K., Maimon, T., Patla, I., Villa, E., and Medalia, O. (2010). Visualizing cellular processes at the molecular level by cryo-electron tomography. *J. Cell Sci.* **123**, 7–12.

Bladen, H.A., and Mergenhagen, S.E. (1964). Ultrastructure of *Veillonella* and Morphological Correlation of an OM with Particles Associated with Endotoxic Activity. *J. Bacteriol.* **88**, 1482–1492.

Blaylock, B., Jiang, X., Rubio, A., Moran, C.P., Jr., and Pogliano, K. (2004). Zipper-like interaction between proteins in adjacent daughter cells mediates protein localization. *Genes Dev.* **18**, 2916–2928.

Bos, M.P., Robert, V., and Tommassen, J. (2007). Biogenesis of the gram-negative bacterial outer membrane. *Annu. Rev. Microbiol.* **61**, 191–214.

Briegel, A., Dias, D.P., Li, Z., Jensen, R.B., Frangakis, A.S., and Jensen, G.J. (2006). Multiple large filament bundles observed in *Caulobacter crescentus* by electron cryotomography. *Mol. Microbiol.* **62**, 5–14.

Briegel, A., Ortega, D.R., Tocheva, E.I., Wuichet, K., Li, Z., Chen, S., Müller, A., Iancu, C.V., Murphy, G.E., Dobro, M.J., et al. (2009). Universal architecture of bacterial chemoreceptor arrays. *Proc. Natl. Acad. Sci. USA* **106**, 17181–17186.

Buchanan, C.E., Henriques, A.O., and Piggot, P.J. (1994). Bacterial cell wall, First Edition, *Volume 1* (New York: Elsevier Science).

Cavalier-Smith, T. (2004). Organelles, genomes, and eukaryote phylogeny: an evolutionary synthesis in the age of genomics (London: CRC Press).

Chart, H., Okubadejo, O.A., and Rowe, B. (1992). The serological relationship between *Escherichia coli* O157 and *Yersinia enterocolitica* O9 using sera from patients with brucellosis. *Epidemiol. Infect.* **108**, 77–85.

Chen, S., Beeby, M., Murphy, G.E., Leadbetter, J.R., Hendrixson, D.R., Briegel, A., Li, Z., Shi, J., Tocheva, E.I., Müller, A., et al. (2011). Structural diversity of bacterial flagellar motors. *EMBO J.* **30**, 2972–2981.

Dmitriev, B.A., Toukach, F.V., Schaper, K.J., Holst, O., Rietschel, E.T., and Ehlers, S. (2003). Tertiary structure of bacterial murein: the scaffold model. *J. Bacteriol.* **185**, 3458–3468.

Doi, R.H. (1989). Sporulation and germination. In *Bacillus*, C.R. Harwood, ed. (London: Plenum), pp. 169–215.

Dowd, M.M., Orsburn, B., and Popham, D.L. (2008). Cortex peptidoglycan lytic activity in germinating *Bacillus anthracis* spores. *J. Bacteriol.* **190**, 4541–4548.

Driks, A. (2002). Maximum shields: the assembly and function of the bacterial spore coat. *Trends Microbiol.* **10**, 251–254.

Edgar, R.C. (2004). MUSCLE: multiple sequence alignment with high accuracy and high throughput. *Nucleic Acids Res.* **32**, 1792–1797.

Erickson, H.P. (2009). Size and shape of protein molecules at the nanometer level determined by sedimentation, gel filtration, and electron microscopy. *Biol. Proced. Online* **11**, 32–51.

Errington, J. (1993). *Bacillus subtilis* sporulation: regulation of gene expression and control of morphogenesis. *Microbiol. Rev.* **57**, 1–33.

Errington, J. (2003). Regulation of endospore formation in *Bacillus subtilis*. *Nat. Rev. Microbiol.* **1**, 117–126.

Gan, L., Chen, S., and Jensen, G.J. (2008). Molecular organization of Gram-negative peptidoglycan. *Proc. Natl. Acad. Sci. USA* **105**, 18953–18957.

Gueiros-Filho, F. (2007). *Bacillus Cellular and Molecular Biology*, First Edition, *Volume 1* (Norfolk, UK: Caister Academic Press).

Gutierrez, J., Smith, R., and Pogliano, K. (2010). SpoIID peptidoglycan hydrolase activity is required throughout engulfment during *Bacillus subtilis* sporulation. *J. Bacteriol.* **192**, 3174–3186.

Hayhurst, E.J., Kailas, L., Hobbs, J.K., and Foster, S.J. (2008). Cell wall peptidoglycan architecture in *Bacillus subtilis*. *Proc. Natl. Acad. Sci. USA* **105**, 14603–14608.

Henriques, A.O., and Moran, C.P., Jr. (2007). Structure, assembly, and function of the spore surface layers. *Annu. Rev. Microbiol.* **61**, 555–588.

Hilbert, D.W., and Piggot, P.J. (2004). Compartmentalization of gene expression during *Bacillus subtilis* spore formation. *Microbiol. Mol. Biol. Rev.* **68**, 234–262.

- Hofstad, T. (1978). Chemotypes of *Veillonella* lipopolysaccharides. *Acta Pathol. Microbiol. Scand. [B]* 86, 47–50.
- Hofstad, T., and Kristoffersen, T. (1970). Chemical composition of endotoxin from oral *Veillonella*. *Acta Pathol Microbiol Scand B Microbiol Immunol* 78, 760–764.
- Iancu, C.V., Tivol, W.F., Schooler, J.B., Dias, D.P., Henderson, G.P., Murphy, G.E., Wright, E.R., Li, Z., Yu, Z., Briegel, A., et al. (2006). Electron cryotomography sample preparation using the Vitrobot. *Nat. Protoc.* 1, 2813–2819.
- Illing, N., and Errington, J. (1991). Genetic regulation of morphogenesis in *Bacillus subtilis*: roles of sigma E and sigma F in prespore engulfment. *J. Bacteriol.* 173, 3159–3169.
- Joseleau-Petit, D., Liébart, J.C., Ayala, J.A., and D'Ari, R. (2007). Unstable *Escherichia coli* L forms revisited: growth requires peptidoglycan synthesis. *J. Bacteriol.* 189, 6512–6520.
- Kane, M.D., and Breznak, J.A. (1991). *Acetonema longum* gen. nov. sp. nov., an H<sub>2</sub>/CO<sub>2</sub> acetogenic bacterium from the termite, *Pterotermes occidentis*. *Arch. Microbiol.* 156, 91–98.
- Komeili, A., Li, Z., Newman, D.K., and Jensen, G.J. (2006). Magnetosomes are cell membrane invaginations organized by the actin-like protein MamK. *Science* 311, 242–245.
- Kremer, J.R., Mastrorade, D.N., and McIntosh, J.R. (1996). Computer visualization of three-dimensional image data using IMOD. *J. Struct. Biol.* 116, 71–76.
- Kuo, C.H., and Ochman, H. (2010). The extinction dynamics of bacterial pseudogenes. *PLoS Genet.* 6, e1001050.
- Lake, J.A. (2009). Evidence for an early prokaryotic endosymbiosis. *Nature* 460, 967–971.
- Leadbetter, J.R., and Breznak, J.A. (1996). Physiological ecology of *Methanobrevibacter cuticularis* sp. nov. and *Methanobrevibacter curvatus* sp. nov., isolated from the hindgut of the termite *Reticulitermes flavipes*. *Appl. Environ. Microbiol.* 62, 3620–3631.
- Li, Z., and Jensen, G.J. (2009). Electron cryotomography: a new view into microbial ultrastructure. *Curr. Opin. Microbiol.* 12, 333–340.
- Liu, J., Lin, T., Botkin, D.J., McCrum, E., Winkler, H., and Norris, S.J. (2009). Intact flagellar motor of *Borrelia burgdorferi* revealed by cryo-electron tomography: evidence for stator ring curvature and rotor/C-ring assembly flexion. *J. Bacteriol.* 191, 5026–5036.
- Margolin, W. (2002). Bacterial sporulation: FtsZ rings do the twist. *Curr. Biol.* 12, R391–R392.
- Mergenhagen, S.E. (1965). Polysaccharide-lipid complexes from *Veillonella parvula*. *J. Bacteriol.* 90, 1730–1734.
- Meyer, P., Gutierrez, J., Pogliano, K., and Dworkin, J. (2010). Cell wall synthesis is necessary for membrane dynamics during sporulation of *Bacillus subtilis*. *Mol. Microbiol.* 76, 956–970.
- Nicholson, W.L., and Setlow, P. (1990). Dramatic increase in negative superhelicity of plasmid DNA in the forespore compartment of sporulating cells of *Bacillus subtilis*. *J. Bacteriol.* 172, 7–14.
- Onyenwoke, R.U., Brill, J.A., Farahi, K., and Wiegel, J. (2004). Sporulation genes in members of the low G+C Gram-type-positive phylogenetic branch (Firmicutes). *Arch. Microbiol.* 182, 182–192.
- Perez, A.R., Abanes-De Mello, A., and Pogliano, K. (2000). SpoIIb localizes to active sites of septal biogenesis and spatially regulates septal thinning during engulfment in *bacillus subtilis*. *J. Bacteriol.* 182, 1096–1108.
- Piggot, P.J., and Hilbert, D.W. (2004). Sporulation of *Bacillus subtilis*. *Curr. Opin. Microbiol.* 7, 579–586.
- Pilhofer, M., Ladinsky, M.S., McDowall, A., and Jensen, G. (2010). Bacterial-TEM: new insights from cryo-microscopy. In *Electron Microscopy of Model Systems*, T. Mueller-Reichert, ed. (Oxford: Elsevier).
- Poindexter, J.S., and Hagenzieker, J.G. (1981). Constriction and septation during cell division in caulobacters. *Can. J. Microbiol.* 27, 704–719.
- Popham, D.L., Helin, J., Costello, C.E., and Setlow, P. (1996). Analysis of the peptidoglycan structure of *Bacillus subtilis* endospores. *J. Bacteriol.* 178, 6451–6458.
- Prajapati, R.S., Ogura, T., and Cutting, S.M. (2000). Structural and functional studies on an FtsH inhibitor from *Bacillus subtilis*. *Biochim. Biophys. Acta* 1475, 353–359.
- Rainey, F. (2009). *Bergey's manual of systematic bacteriology*, Second Edition, Volume 3 (New York: Springer).
- Ramamurthi, K.S., and Losick, R. (2008). ATP-driven self-assembly of a morphogenetic protein in *Bacillus subtilis*. *Mol. Cell* 31, 406–414.
- Ramamurthi, K.S., and Losick, R. (2009). Negative membrane curvature as a cue for subcellular localization of a bacterial protein. *Proc. Natl. Acad. Sci. USA* 106, 13541–13545.
- Ramamurthi, K.S., Clapham, K.R., and Losick, R. (2006). Peptide anchoring spore coat assembly to the outer forespore membrane in *Bacillus subtilis*. *Mol. Microbiol.* 62, 1547–1557.
- Ramamurthi, K.S., Lecuyer, S., Stone, H.A., and Losick, R. (2009). Geometric cue for protein localization in a bacterium. *Science* 323, 1354–1357.
- Roels, S., Driks, A., and Losick, R. (1992). Characterization of spoIIA, a sporulation gene involved in coat morphogenesis in *Bacillus subtilis*. *J. Bacteriol.* 174, 575–585.
- Sabatini, D.D., Bensch, K., and Barmett, R.J. (1963). Cytochemistry and electron microscopy. The preservation of cellular ultrastructure and enzymatic activity by aldehyde fixation. *J. Cell Biol.* 17, 19–58.
- Setlow, P. (2007). I will survive: DNA protection in bacterial spores. *Trends Microbiol.* 15, 172–180.
- Setlow, P. (2008). Dormant spores receive an unexpected wake-up call. *Cell* 135, 410–412.
- Smith, T.J., Blackman, S.A., and Foster, S.J. (2000). Autolysins of *Bacillus subtilis*: multiple enzymes with multiple functions. *Microbiology* 146, 249–262.
- Steichen, C.T., Kearney, J.F., and Turnbough, C.L., Jr. (2007). Non-uniform assembly of the *Bacillus anthracis* exosporium and a bottle cap model for spore germination and outgrowth. *Mol. Microbiol.* 64, 359–367.
- Stevens, C.M., Daniel, R., Illing, N., and Errington, J. (1992). Characterization of a sporulation gene, spoIIA, involved in spore coat morphogenesis in *Bacillus subtilis*. *J. Bacteriol.* 174, 586–594.
- Tipper, D.J., and Linnett, P.E. (1976). Distribution of peptidoglycan synthetase activities between sporangia and forespores in sporulating cells of *Bacillus sphaericus*. *J. Bacteriol.* 126, 213–221.
- Yanouri, A., Daniel, R.A., Errington, J., and Buchanan, C.E. (1993). Cloning and sequencing of the cell division gene pbpB, which encodes penicillin-binding protein 2B in *Bacillus subtilis*. *J. Bacteriol.* 175, 7604–7616.